

AUV Trajectory Learning for Underwater Acoustic Energy Transfer and Age Minimization

Mohamed Afouene Melki, Mohammad Shehab, and Mohamed-Slim Alouini

Abstract—Internet of underwater things (IoUT) is increasingly gathering attention with the aim of monitoring sea life and deep ocean environment, underwater surveillance as well as maintenance of underwater installations. However, conventional IoUT devices, reliant on battery power, face limitations in lifespan and pose environmental hazards upon disposal. This paper introduces a sustainable approach for simultaneous information uplink from the IoUT devices and acoustic energy transfer (AET) to the devices via an autonomous underwater vehicle (AUV), potentially enabling them to operate indefinitely. To tackle the time-sensitivity, we adopt age of information (AoI), and Jain's fairness index. We develop two deep-reinforcement learning (DRL) algorithms, offering a high-complexity, high-performance frequency division duplex (FDD) solution and a low-complexity, medium-performance time division duplex (TDD) approach. The results elucidate that the proposed FDD and TDD solutions significantly reduce the average AoI and boost the harvested energy as well as data collection fairness compared to baseline approaches.

Index Terms—Age of Information, deep reinforcement learning, energy efficiency, sustainability, AUVs, acoustic energy transfer

I. INTRODUCTION

The health of our planet relies heavily on the well-being of its oceans, which serve as vital sources of oxygen, sustenance, and energy. Communication in extreme environments such as seas and deep oceans is of paramount importance due to its role in search and rescue operations, surveillance, maintenance of optical fibers and gas pipelines, and environmental monitoring among many other applications [1], [2]. Each application has specific requirements in terms of communication range, energy consumption, data rate, and latency tolerance. Over time, underwater connectivity is becoming more vital.

The Internet-of-Underwater-Things (IoUTs), a global network connecting underwater objects, facilitates continuous monitoring of oceans. This network generates high-resolution data essential for training machine learning (ML) algorithms to swiftly evaluate potential climate change solutions and aid in decision-making processes. In addition, recent advances highlighted the potential of IoUT for underwater localization [3] and the defense against attacks for such localization approaches [4]. Furthermore, and within the efforts leading to enhanced underwater connectivity for divers, the authors of [5] developed the world's first underwater wifi "AquaFi" to transfer data from a diver's smartphone to a gateway

This work is supported by the KAUST Office of Sponsored Research under Award ORA-CRG2021-4695.

The authors are with CEMSE Division, King Abdullah University of Science and Technology (KAUST), Thuwal 23955-6900, Saudi Arabia (emails: mohamed.melki@kaust.edu.sa, mohammad.shehab@kaust.edu.sa, slim.alouini@kaust.edu.sa).

device mounted on their equipment. This gateway then relays the data through a light beam to a surface computer, which is connected to the internet via satellite. However, the light beam is only suitable for short distances and suffers from disruptions due to tides and underwater movements. In response to these limitations, recent advancements have explored alternative acoustic approaches to achieve long-range, low-power underwater communication. For instance, the work in [6] presents an underwater backscatter communication system that enables long-distance communication by encoding data in sound waves reflected back to a receiver. Tested in river and ocean environments, this system demonstrated a significantly greater communication range than previous technologies, while maintaining low power consumption, marking a substantial improvement for sustained underwater connectivity.

Due to their ability to navigate freely and reach remote and risky locations for divers, AUVs are considered to be a very attractive solution for gathering information from IoUT devices. In this context, the work in [7] illustrated the application of federated learning in collaborative information processing via AUVs in IoUT. Nevertheless, the nature of underwater communication is different from other environments. For instance, conventional IoUT sensors, reliant on battery power, face limitations in lifespan, difficulties with battery replacement, and pose environmental hazards upon disposal. Unlike terrestrial systems, underwater communication suffers from significant signal attenuation, tidal turbulence and multi-path effects. These challenges necessitate innovative approaches to optimize the paths of AUVs for effective data collection and wireless energy transfer.

Understanding and overcoming the limitations of communication in underwater environments can lead to more robust and efficient systems, paving the way for future innovation in the field. In this context, the work in [8], [9] presented a comprehensive summary on different communication and energy transfer technologies underwater. However, no single technology can meet all requirements across different activities simultaneously. Hence, each system is tailored to suit specific applications. According to their discussion and many other works such as [10], it is evident that despite the drawback of low data rates and slow propagation, the adoption of acoustic transmission is superior to optical transmission and magnetic induction in terms of resilience and long range. This is further elaborated in [10], where the attenuation coefficients for magnetic induction and electromagnetic-based energy transfer are too high compared to AET. This in turn affects the efficiency of energy transmission causing a great loss when the distance of energy transfer is longer than few meters.

This preference is further supported in [11], which provides a comparative analysis of both commercial and research acoustic modems. This study highlights the modem parameters crucial for underwater applications, such as operating range, data rate, modulation schemes, and power consumption, identifying current trends and key design challenges. Additionally, the survey in [12] emphasizes the importance of acoustic technology for underwater communication systems, particularly as underwater IoT devices typically transmit small, delay-tolerant data packets such as sensor readings, making acoustic technology well-suited for our endeavor. Despite the infancy of the idea of underwater AET, an example of new advances in hardware design for AET can be found in [13], which illustrates transducer structure for underwater AET system.

Assuming instant reception, AoI is defined as the time elapsed since the reception of the last information update from an IoT device [14], [15]. AoI minimization is of paramount importance since the lower the AoI, the fresher the information received from a specific IoT device. A lot of research has been conducted on applying machine learning in order to minimize the AoI of devices in above-water environments. For instance, the authors of [16] applied deep reinforcement learning (DRL) to design the trajectory of UAV collecting information from a small number of grounded devices with the goal of minimizing the AoI of these devices. Moreover, the study in [17] explored the use of multiple Unmanned Aerial Vehicles (UAVs) to optimize both AoI and power consumption of a relatively larger number of devices. In [18], the same authors expanded their setup further, where a swarm of UAVs collects data from device clusters constituting a massive IoT network. These efforts highlight the importance of efficient path planning, scheduling, and power management to ensure timely data collection and energy efficiency.

To this end, authors generally resorted to RL due to the high complexity and dimensionality of the trajectory optimization problem in such cases, especially when taking the energy and environmental details into consideration. In particular, when dealing with problems of high dimensional state and action spaces, DRL is known for its efficiency. This is because DRL is able to sample and reduce the dimensionality of those spaces, which renders a faster, yet highly sub-optimal solution. Similar research in underwater environments remains sparse. This area has not been extensively studied until Omoke et al. [19] published the first attempt to apply RL to perform simultaneous wireless power transfer and data collection in an underwater system. They demonstrated relatively good results, despite their setup being somewhat similar to terrestrial systems, where a vehicle needs to get very close to devices to power them up and exchange data. However, their model did not account for AoI and its trade-off with the energy harvesting goal.

Hence, the exploration of RL in underwater environments is crucial due to the unique challenges posed by underwater communication and navigation. In this context, the authors of [20] presented a wide discussion on how RL could help tackle IoT challenges. The online nature of RL was shown to be well-tailored to the dynamic nature of underwater channel, link outages, bandwidth allocation as well as AUV control

problems. Moreover, in [21], Dai et al. proposed an RL approach for underwater relay selection and power control. By focusing on RL to optimize AUV trajectories, this work aims to address the challenge of battery-constrained IoT and information uplink, which contributes to the advancement of underwater wireless communication technologies. We assume a set of underwater IoT devices that rely mainly on harvested energy from acoustic sources to transmit information. The target is to optimize the underwater AUV trajectory and device scheduling in order to minimize the average AoI and implicitly maximize the harvested energy via AET.

A. Contributions

The motivation behind this work stems from its novelty in accounting for AoI minimization and solving the problem of battery replacement for IoT devices. This leads to avoiding hazardous material underwater, which might affect sea life. Our research also complements the acoustic communication system in a sustainable framework. Particularly, in the context of planning paths and scheduling for underwater simultaneous wireless communication and energy transfer, the contributions of this paper are summarized as follows:

- With the goal of minimizing the average weighted AoI of IoT devices, we develop a couple of DRL solutions for AUV trajectory planning for simultaneous AET and information uplink
- The first approach is FDD-based high performance, high complexity, and two antenna-based solution.
- The second one is a TDD-based low complexity, low-cost alternative solution that adopts only one antenna for both AET and information reception and the AUV.
- Compared to baseline approaches such as random walk (RW), round robin (RR), and the greedy algorithm (GA), the proposed FDD and TDD DRL-based approaches jointly minimize the AoI and maximize the harvested energy and data collection fairness at the IoT devices.

B. Outline

The rest of the paper is organized as follows: Section II describes the system model and basic information about underwater communication. Next, Section III formulates the simultaneous AET and information uplink problem and elucidates TDD and FDD. Section IV proposes the DRL-PPO, while Section V depicts the experimental results. Finally, Section VI concludes the paper. The appendices include some mathematical proofs and derivations that serve the solution of the presented optimization problem.

II. SYSTEM MODEL

A. Network Model

As illustrated in Fig. 1, we consider an IoT network, comprising an AUV deployed from a surface buoy station, and K IoT nodes dispersed randomly in a 3-D underwater space. Each IoT device k is spatially distributed across the 3D equally spaced grid world and is assigned fixed coordinates $c_k = (x_k, y_k, z_k)$. Similarly, at time t the AUV is designated

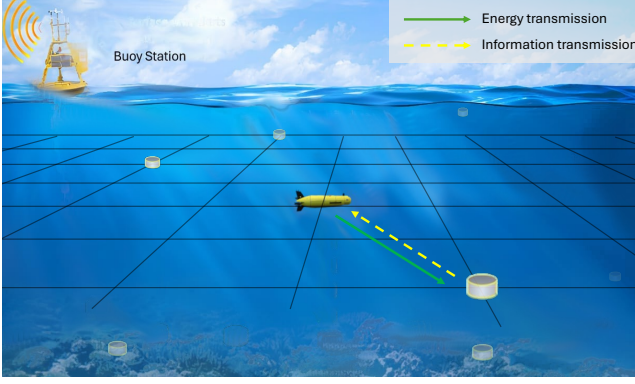


Fig. 1. AUV and IoUT network in the underwater grid world

coordinates $l_{auv}(t) = (x_{auv}(t), y_{auv}(t), z_{auv}(t))$. Each IoUT device is equipped with sensors designed for monitoring essential underwater parameters such as temperature, pH level, and dissolved oxygen concentration. The AUV maneuvers through the grid world to establish communication with the underwater sensor nodes, where communication is facilitated through an acoustic modem/hydrophone. Moreover, as the AUV traverses the network, it employs AET to provide energy, thereby recharging energy-constrained IoUT nodes.

B. Channel Model

In acoustic communication, the received level (RL) in dB at an IoUT device that is located at distance d from the source (i.e., AUV) is calculated as [22]

$$RL = SL - AL - NL, \quad (1)$$

where SL is the acoustic source level, AL characterizes the total attenuation level and NL is the ambient noise level. The SL of an underwater acoustic transmitter is given by

$$SL = 170.8 + 10 \log_{10} P_{elec} + 10 \log_{10} \eta + DI, \quad (2)$$

where DI is the directivity index of the source in dB, P_{elec} is the electrical input power at the source, while the electro-acoustic power conversion efficiency η varies between 0.2 and 0.7 for practical modems.

Assuming deep water characteristics and neglecting reflection from the air and bottom surfaces throughout the analysis, combining absorption, channel spreading loss, and noise, the total attenuation level (AL) in dB is given by¹

$$AL = k_s \cdot 10 \log_{10} d + d \cdot 10 \log_{10} \alpha(f), \quad (3)$$

where and k_s is the spreading factor that takes the value of 1 or 2 depending on the assumptions; $k_s = 2$ is referred to as spherical spreading experienced when a sound wave propagates away from the source uniformly in 3 directions, when $d <$ water depth. Meanwhile, $k_s = 1$ is referred to as cylindrical spreading experienced when the acoustic signal systematically hits the sea surface and sea floor before reaching the destination. $\alpha(f)$ is the absorption coefficient of

¹For simplicity and focusing on the main system optimization, we assumed flat fading

acoustic waves underwater that can be expressed using Thorp's formula for frequencies above a few hundred Hz, [10]

$$\alpha(f) = 0.11 \frac{f^2}{f^2 + 1} + 44 \frac{f^2}{f^2 + 4100} + 2.75 \times 10^{-4} f^2 + 0.003, \quad (4)$$

where f is the acoustic transmission frequency.

III. PROBLEM FORMULATION

A. Acoustic Energy Transfer and Information Uplink

1) *Acoustic Energy Transfer*: The process of AET begins with the emission of acoustic waves by the AUV through its hydrophone. These waves carry transmitted power and propagate as fluctuating pressure waves characterized by their amplitude, frequency, and phase. Subsequently, the IoUT nodes' hydrophones receive these energy waves. The process also involves the use of transducers that can convert acoustic pressure waves into electrical energy. This electrical energy is then stored in a battery onboard the IoUT node. The pressure fluctuations can be expressed as [22]

$$p = 10^{RL/20}. \quad (5)$$

The fluctuations generate a voltage at its open circuit terminals as mentioned earlier. The receiving voltage sensitivity (RVS) of a hydrophone is defined as [22]

$$RVS = 20 \log_{10} M, \quad (6)$$

where M is the sensitivity in $V/\mu Pa$. Using (5) and (6), the induced voltage, at the receiver hydrophone terminals V_{ind} is given by

$$V_{ind} = p \cdot M = 10^{\frac{RL+RVS}{20}}. \quad (7)$$

The electrical power available for harvesting, $P_{available}$ depends on the impedance matching between the receiver hydrophone and the surrounding seawater. For a single hydrophone, this can be expressed as

$$P_{available} = \frac{V_{ind}^2}{4R_p}, \quad (8)$$

where R_p is the load resistance required to ensure impedance matching. This gives us the total harvestable power, which is given by

$$P_{harv} = \eta \cdot P_{available} = \eta \cdot \frac{10^{(RL+RVS)/10}}{4R_p}, \quad (9)$$

where η is the acoustic-electric power conversion efficiency. Then, the energy harvested is calculated as

$$E_{harv} = P_{harv} \cdot \tau_{charging}, \quad (10)$$

where $\tau_{charging}$ represents the time taken by the AUV to transmit energy to the IoUT node.

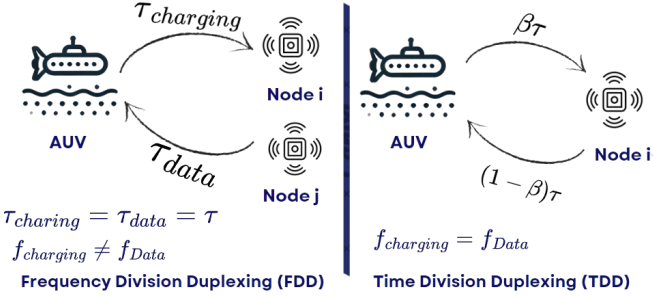


Fig. 2. AET and information uplink using FDD vs TDD

2) *Information Uplink*: During the communication between the IoT nodes and the AUV, the latter collects data. The SNR, γ_k between the k^{th} node and the AUV can be expressed as

$$\gamma_k = 2^{(S/B)} - 1, \quad (11)$$

where S is the system throughput and B is the bandwidth. The transmit power of the k^{th} node $P_{trans,k}$ is [19]

$$P_{trans,k} = \gamma_k \cdot 10^{\frac{NL}{10}} \cdot 10^{\frac{AL_{k,auv}}{10}}, \quad (12)$$

where $AL_{k,auv}$ is the transmission loss between the k^{th} node and the AUV. The energy required by a node k to transmit information to the AUV is

$$E_{req,k} = P_{trans,k} \cdot \tau_{data}, \quad (13)$$

where τ_{Data} is the time required to transmit the payload from the sensor to the AUV.

3) *Age Of Information*: Upon transmission of a packet by a selected IoT device k at time step t , its AoI $A_k(t)$ resets to 1, which indicates that fresh information has just been received from that device.

B. Duplexing Techniques

In underwater simultaneous communication and AET, duplexing techniques play a crucial role in determining the efficiency and effectiveness of data and energy transmission. Herein, we adopt two primary types of duplexing, namely FDD and TDD. Each technique has its own set of advantages and challenges as noted in [23], which impacts their applicability in various circumstances. The two techniques are illustrated in Fig. 2

1) *Frequency-Division Duplexing*: FDD is a duplexing method where separate frequency bands are allocated for AET and information uplink. This means that AET and data transmission can occur simultaneously but on different frequencies. FDD is particularly useful in scenarios where separate and large uplink and downlink bandwidth requirements are needed, providing continuity and high capacity for energy and information transmission with limited interference. As shown in the left part of Fig. 2, the AUV utilizes two distinct frequency bands with different central frequencies $f_{charging}$ for AET to i^{th} node and f_{data} for data uplink from j^{th} node. This separation of frequencies ensures that the two processes can

occur without interference. In our case, FDD can be advantageous due to its ability to handle simultaneous bidirectional AET and information uplink, reducing latency and improving throughput. However, the need for separate frequency bands can lead to spectrum inefficiency, as it requires a broader range of frequencies to operate. Additionally, the hardware complexity increases because of the necessity for duplexers as well as multiple antennas to separate the data and AET at the transmitter and receiver.

2) *Time-Division Duplexing*: TDD is a method where the same frequency band is used for both AET and information uplink but at different times. This technique involves switching between transmitting and receiving modes within designated time slots, effectively utilizing the same frequency spectrum for both operations. TDD is particularly useful in scenarios where limited hardware and frequency resources exist, allowing for dynamic adjustment of AET and information uplink based on real-time demand. As shown in the right part of Fig. 2, the AUV shares the same frequency band for AET and data uplink but allocates different durations for each operation. The total communication duration τ is divided into $\beta\tau$ for AET and $(1 - \beta)\tau$ for data uplink, where β represents the time-splitting factor. This allocation ensures efficient use of the available spectrum by sequentially performing energy transfer and data communication. TDD is advantageous in the sense of its efficient spectrum usage and flexibility. It simplifies the hardware design by eliminating the need for separate frequency bands, antennas, and duplexers. However, precise time synchronization is crucial to avoid interference between data uplink and energy downlink transmissions.

C. Problem Formulation

Inspired by existing works such as [16], [18], and [24] which focus on minimizing the AoI and improving fairness in UAV-based communication systems, we extend these concepts to address the specific challenges in AUVs. To minimize the weighted average AoI of collected data, the AUV trajectory planning problem can be formulated as follows²

$$\begin{aligned} \mathbf{P1:} \quad & \min_{\{x_k(t)\}_{t=0}^T, \{l_{auv}(t)\}_{t=0}^T} \frac{(1 - \mathcal{J}_T)}{T} \cdot \sum_{t=1}^T \frac{1}{K} \sum_{k=1}^K \delta_k \cdot A_k(t) \\ & \text{Subject to:} \quad A_k(t) \leq A_{\max}, \quad \forall k, \forall t \\ & \quad \mathcal{J}_T \geq \mathcal{J}_{\min} \\ & \quad x_k(t) \cdot e_k(t) \geq x_k(t) E_{req,k}(t), \forall k, \forall t \\ & \quad \sum_{k=1}^K x_k(t) = 1, \quad \forall t \\ & \quad x_k(t) \in \{0, 1\}, \quad \forall k, \forall t \\ & \quad l_{auv}(t) \in \mathcal{X}, \quad \forall t \end{aligned}$$

In this formulation, δ_k represents the importance weight assigned to device k and A_{\max} is the maximum allowed AoI in the system. The binary variable x_k indicates whether device k

²In this problem formulation, we focus on the communication between the AUV and sensor nodes. The dynamics of the AUV and its energy consumption are beyond the scope of this work. For simplicity, we assume the AUV has sufficient energy throughout the entire navigation time.

is selected for data transmission ($x_k = 1$) or not ($x_k = 0$). The energy stored in device k at time t is denoted by $e_k(t)$, while $E_{\text{req},k}(t)$ represents the minimum energy required for device k to transmit data. The constraint $x_k \cdot e_k(t) \geq x_k \cdot E_{\text{req},k}(t)$ ensures that the selected device has enough energy to transmit. The condition $\sum_{k=1}^K x_k = 1$ enforces that only one device is selected at each time step. Finally, the constraint $l_{\text{aUV}}(t) \in \mathcal{X}$ ensures that the AUV remains within the defined grid world, where \mathcal{X} denotes the set of all possible locations within the grid.

The weighted average AoI, as expressed in the objective function, allows assigning varying levels of importance to different nodes. This is particularly useful in scenarios involving critical and non-critical nodes, where higher priority can be given to nodes with stricter data freshness requirements [25]. In this work, we simplify the analysis by setting all weights δ_k to 1, ensuring that all nodes are treated equally in terms of importance. This assumption allows us to focus on evaluating the overall performance of the proposed approach without introducing additional bias in the optimization objective.

The main objective of problem **P1** is to minimize the average AoI. To achieve this, the solution should ensure that sufficient energy is available at each IoUT node for data transmission, which implicitly maximizes the harvested energy. However, this approach may lead to an unfair distribution of data collection among devices despite boosting the overall global performance. To address this issue, we make use of Jain's fairness index, \mathcal{J}_T , as a metric to ensure fair data gathering [24]. This index is defined based on the frequency of data collection from each device over a period T , where

$$\mathcal{J}_T = \frac{\left(\sum_{k=1}^K D_T(k)\right)^2}{K \sum_{k=1}^K D_T(k)^2}, \quad (15)$$

where $D_T(k)$ denotes the total number of times the data was collected from the device k over the period T . The value of \mathcal{J}_T lies within the range $[0, 1]$, and it can be interpreted as follows:

- If \mathcal{J}_T is close to 1, it indicates that all nodes are receiving equal attention during data collection, meaning the data collection process is balanced and fair.
- If \mathcal{J}_T is close to 0, it implies an unbalanced distribution where some nodes are prioritized significantly more than others, leading to neglect of certain nodes.

In the context of this work, Jain's fairness index ensures that no IoUT node is overly prioritized or ignored, even as the global performance (e.g., minimizing AoI) is optimized. By monitoring \mathcal{J}_T , we achieve a balance between performance and fairness, which is crucial in applications where uniform data collection across nodes is essential.

In our problem, we aim to maximize Jain's fairness index. Moreover, this index is not allowed to fall below a specific threshold \mathcal{J}_{\min} to guarantee a reasonable amount of fairness on data collection.

In summary, our objective is to simultaneously achieve fair data gathering and minimize the average AoI. Given the complexity and NP-hard nature of this problem, traditional

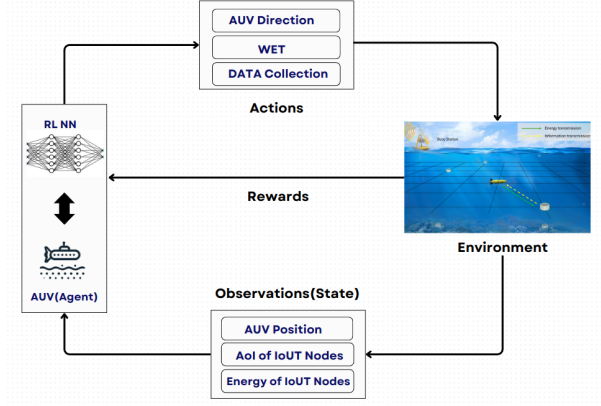


Fig. 3. The interaction between the agent and the environment

optimization techniques are impractical. To model the association and interaction pattern between the AUV and IoUT devices, the AUV trajectory planning problem is formulated as a Markov decision process (MDP) that captures the dynamics of the AUV. DRL is employed for this MDP due to its ability to manage large state and action spaces and adapt to complex, nonlinear systems, robustly optimizing the AUV's trajectory while ensuring energy-efficient communication and fair data collection across the network.

IV. THE PROPOSED DRL SOLUTION

A. Markov Decision Process Formulation

We formulate the problem as an MDP that is defined by the tuple $\langle \mathcal{S}, \mathcal{A}, R, P \rangle$, where \mathcal{S} is the state space, \mathcal{A} represents the action space, R denotes the reward function. We consider a finite horizon MDP with a probabilistic state transition function $P : \mathcal{S} \times \mathcal{A} \times \mathcal{S} \rightarrow \mathbb{R}$. At time instant t , the agent (AUV) observes the current state $s(t)$ from the environment and tries to follow the optimal policy by selecting the best action $a(t)$, which maximizes the reward $r(t)$ and transiting to the next state $s(t+1)$ with a probability $p(s(t), s(t+1))$. The agent can then rely on these policies to make all future data transfer and AET decisions as illustrated in Fig. 3. For convenience, we propose an episodic MDP. This means that the AUV's data collection and energy transmission is over at time $T \in \mathbb{N}$, where the total navigation time T is dictated by the amount of navigation energy available at the AUV and the dimensions of the network. Time slots are discretely divided as $t = \{\tau, 2\tau, \dots, T\}$, where τ is the time that the AUV takes to move from one grid point to another adjacent one. τ is dictated by the AUV's velocity and the spacing between grids.

1) *State space:* The state space of the system at time slot t is defined as $s(t) = (l_{\text{aUV}}(t), A(t), \mathcal{E}(t))$, where $l_{\text{aUV}}(t)$ is a vector containing the current position of the AUV at time slot t . $A(t)$ is a vector that contains the current AoI of all the IoUT devices at time slot t , where $A_k(t) \in \mathcal{I} = [1, 2, \dots, A_{\max}]$ and A_{\max} is the maximum allowed AoI in the model, which is chosen to be arbitrarily high. $\mathcal{E}(t)$ represents a vector of the available energy at each IoUT node, which belongs to a discrete set \mathcal{E} . Without loss of generality, we will consider

the discrete 3D coordinates of the AUV and IoUT to be integers to reduce the computational demand of representing the system state. Note that the state is updated before being fed to the agent. Considering the three described components, the dimensionality of the state space could be described as

$$S = \underbrace{X^3}_{\text{Auv Position}} \times \underbrace{\mathcal{E}^K}_{\text{Energy Stored}} \times \underbrace{I^K}_{\text{Device age of information}}, \quad (16)$$

Remark 1. *These components were selected to capture the critical spatial ($l_{\text{auv}}(t)$), temporal ($A(t)$), and energy ($\mathcal{E}(t)$) dynamics of the system, enabling the agent to make informed decisions for AoI minimization and fairness. Excluding $\mathcal{E}(t)$ from the state space results in failed data transmissions, as the agent is unable to account for energy availability at the nodes. Similarly, removing $A(t)$ leads to poor AoI optimization, as the agent lacks awareness of data freshness.*

2) *Action space:* We have developed two approaches for defining the action space in our RL framework: a 3D action space for FDD communication and a 2D action space for TDD communication.

First Approach: 3D Action Space (FDD)

The AUV action at time slot t is defined as $a(t) = (d(t), W(t), I(t))$, where $d(t)$ represents the movement of the AUV in a given direction, $W(t) = (w_1(t), w_2(t), \dots, w_K(t))$ is a sparse vector representing the node chosen for WET with $w_k(t) = 1$ indicating that node k is selected, and $I(t) = (i_1(t), i_2(t), \dots, i_K(t))$ is a sparse vector representing the node chosen for Information transmission with $i_k(t) = 1$ indicating that node k is selected for information uplink. The action space is given by:

$$\mathcal{A} = \underbrace{\mathbb{D}^1}_{\text{direction}} \times \underbrace{\{0, 1\}^K}_{\text{sparse vector for WET}} \times \underbrace{\{0, 1\}^K}_{\text{sparse vector for data collection}}, \quad (17)$$

where \mathbb{D} is the direction of movement that can be right, left, up, down, forward, or backward. In this approach, the AUV uses different bands (i.e., central frequencies) for AET and information uplink via two separate antennas, which allows simultaneous operation with different devices.

Second Approach: 2D Action Space (TDD)

To simplify decision-making and reduce computational and hardware demands, TDD reduces the action space to two decisions. The AUV selects a direction for movement and selects the same node for both AET and information uplink, with a portion of the time $\beta\tau$ dedicated to charging and $(1-\beta)\tau$ to data collection. Thus, the TDD action space is defined as:

$$\mathcal{A} = \underbrace{\mathbb{D}^1}_{\text{direction}} \times \underbrace{\{0, 1\}^K}_{\text{sparse vector for node selection}}, \quad (18)$$

Remark 2. *The action space components were chosen to allow the agent to balance AoI reduction, energy replenishment, and efficient navigation. By independently selecting nodes for WET ($W(t)$) and data collection ($I(t)$) in the FDD approach, or combining them into a single node decision in the TDD approach, the framework enables efficient decision-making while accounting for the trade-offs between performance and complexity. Reducing the dimensionality of the*

action space in the FDD approach simplifies decision-making but compromises performance, as the agent loses the ability to independently optimize WET and data collection.

where the sparse vector indicates the IoUT device selected for both AET and information, with the k -th position in the vector being 1 if node k is selected. In that case, $w_k(t) = i_k(t) = 1$.

3) *Transition probability:* The transition between states relies on the 3 components of the state space and the components of the action space. The AoI is updated as follows

$$A_k(t+1) = \begin{cases} 1, & \text{if } i_k(t+1) = 1, \\ A_k(t) + 1, & \text{otherwise,} \end{cases} \quad (19)$$

where $i_k(t+1)$ is the element of the sparse vector $I(t+1)$. The position of the AUV $l_{\text{auv}}(t)$ is updated according to the selected action $d(t)$

$$l_{\text{auv}}(t+1) = \begin{cases} l_{\text{auv}}(t) + (d_g, 0, 0), & d(t) = \text{right}, \\ l_{\text{auv}}(t) - (d_g, 0, 0), & d(t) = \text{left}, \\ l_{\text{auv}}(t) + (0, d_g, 0), & d(t) = \text{up}, \\ l_{\text{auv}}(t) - (0, d_g, 0), & d(t) = \text{down}, \\ l_{\text{auv}}(t) + (0, 0, d_g), & d(t) = \text{forward}, \\ l_{\text{auv}}(t) - (0, 0, d_g), & d(t) = \text{backward}, \end{cases} \quad (20)$$

where d_g is the unit distance between two squares in the grid. As for the energy stored at each node, the update in a node k is as follows

$$\mathcal{E}_k(t+1) = \begin{cases} \mathcal{E}_k(t) + e_r(t) - e_c(t), & \text{if } w_k(t+1) = i_k(t+1) = 1, \\ \mathcal{E}_k(t) + e_r(t), & \text{if only } w_k(t+1) = 1, \\ \mathcal{E}_k(t) - e_c(t), & \text{if only } i_k(t+1) = 1, \\ \mathcal{E}_k(t), & \text{otherwise,} \end{cases} \quad (21)$$

where $e_r(t)$ is the energy received by the node from the AUV at time slot t and $e_c(t)$ is the energy consumed for transmission of the data.

4) *Reward function:* The reward system is defined to minimize the weighted sum of the AoI for all IoUT devices and to maximize Jain's fairness index. For mathematical convenience, we consider the discrimination index instead of the fairness that is defined in (15)

$$\mathcal{D}_T = 1 - \mathcal{J}_T = 1 - \frac{\left(\sum_{k=1}^K D_T(k)\right)^2}{K \sum_{k=1}^K D_T(k)^2}. \quad (22)$$

Herein, maximizing Jain's fairness index is equivalent to minimizing Jain's discrimination index. We define the immediate reward r_u for the AUV at time instant t as

$$r_u(t) = - \left(\frac{\mathcal{D}_t}{K} \sum_{k=1}^K \delta_k A_k(t) + \rho(t) \right), \quad (23)$$

with $\rho(t)$ being the penalty term that varies based on the action space as follows

$$\rho(t) = \rho_{\text{location}}(t) + \rho_{\text{information}}(t) + \rho_{\text{occurrence}}(t), \quad (24)$$

where $\rho_{\text{location}}(t)$ is a penalty applied if the AUV is outside the designated set of valid locations \mathcal{X} . It is defined as

$$\rho_{\text{location}}(t) = \begin{cases} \rho_{\text{loc}}, & \text{if } l_{\text{aau}}(t) \notin \mathcal{X}, \\ 0, & \text{otherwise.} \end{cases} \quad (25)$$

$\rho_{\text{occurrence}}(t)$ is applied to avoid a scenario where a specific node k communicates with the AUV more frequently than others. The number of times node k has been selected to transmit information to the AUV by timeslot t is denoted by $OCC(k, t)$. The penalty is incurred if, at timeslot t , the occurrence $OCC(k, t)$ is higher than the average communication time per node. Since T is the total navigation time of the AUV, $\frac{T}{K}$ represents the ideal number of times each node would send data to the AUV if all nodes were selected equally. The penalty is defined as

$$\rho_{\text{occurrence}}(t) = \begin{cases} \rho_{\text{occ}}, & \text{if } OCC(k, t) > \frac{T}{K}, \\ 0, & \text{otherwise.} \end{cases} \quad (26)$$

The penalty terms $\rho_{\text{location}}(t)$ and $\rho_{\text{occurrence}}(t)$ are the same for both FDD and TDD.

Penalty Term $\rho_{\text{information}}(t)$ for 3D Action Space (FDD)

This penalty is incurred when either no node is available to transmit data or the AUV makes an incorrect selection of a node for data collection. Let $\mathcal{I}(t)$ denote the indices of the nodes that have sufficient energy to transmit data at timeslot t . The penalty is defined as:

$$\rho_{\text{information}}(t) = \begin{cases} \rho_{\text{no_indices}}, & \text{if } \mathcal{I}(t) = \emptyset, \\ \rho_{\text{wrong_indice}}, & \text{if } k \notin \mathcal{I}(t) \text{ and } \mathcal{I}(t) \neq \emptyset, \\ 0, & \text{otherwise.} \end{cases} \quad (27)$$

If no nodes have sufficient energy to transmit data ($\mathcal{I}(t) = \emptyset$), a penalty $\rho_{\text{no_indices}}$ is applied. If there exist nodes with sufficient energy ($\mathcal{I}(t) \neq \emptyset$), but the AUV selects a node that lacks energy for transmission, a penalty $\rho_{\text{wrong_indice}}$ is applied.

Penalty Term $\rho_{\text{information}}(t)$ for 2D Action Space (TDD)

This penalty is introduced to account for situations where simultaneous AET and information uplink do not occur. That is, when the AUV is either only charging (i.e., IoUT node does not have enough energy to transmit data) or only collecting data (IoUT node has sufficient energy to transmit data without getting charged), rather than doing both. The penalty term is defined as

$$\rho_{\text{information}}(t) = \begin{cases} \rho_{\text{only_charging}}, & \text{if } \beta = 1, \\ \rho_{\text{only_transmitting}}, & \text{if } \beta = 0, \\ 0, & \text{otherwise.} \end{cases} \quad (28)$$

B. DRL Solution: Proximal Policy Optimization

Proximal Policy Optimization (PPO) is a mix of two methods: a gradient-based policy that aims to maximize the reward through gradient descent and an actor-critic approach frequently utilized in RL. PPO stands out for its insensitivity to perturbations, a trait it addresses by constraining updates to the neural network. This is achieved by performing updates based on the ratio of the probability of the new policy to the old one. Additionally, PPO considers an advantage function to evaluate

the value of each state [26]. By prioritizing profitable states while controlling the loss function, PPO employs techniques like clipping and setting a lower bound using a minimum function. One distinguishing feature of PPO is its approach to memory management. Instead of storing and sampling from millions of transitions randomly, PPO maintains a fixed-length trajectory of memories, simplifying the process.

The actor is responsible for the actions of the agent based on a learned policy that aims to minimize the clipped loss function defined as [26]

$$L^{CLIP}(\theta) = \hat{\mathbb{E}}_t \left[\min \left(r_t(\theta) \hat{A}_t, \text{clip}(r_t(\theta), 1-\epsilon, 1+\epsilon) \hat{A}_t \right) \right], \quad (29)$$

where $r_t(\theta)$ denotes the probability ratio $r_t(\theta) = \frac{\pi_\theta(a_t|s_t)}{\pi_{\theta_{\text{old}}}(a_t|s_t)}$. Herein, $\pi_\theta(a_t|s_t)$ is the new policy's probability of taking action a_t in state s_t , and $\pi_{\theta_{\text{old}}}(a_t|s_t)$ is the old policy's probability of taking action a_t in state s_t . The term $\text{clip}(r_t(\theta), 1-\epsilon, 1+\epsilon)$ is used to clip the ratio $r_t(\theta)$ between the lower and upper bounds of $1-\epsilon$ and $1+\epsilon$, respectively. The hyperparameter ϵ determines the extent of the clipping, and $\epsilon \approx 0.2$ is the most common value selected in the literature. The objective is to maximize the clipped advantage function, which is a surrogate for the true advantage function \hat{A}_t . The advantage function is defined as

$$\hat{A}_t = -V(s_t) + r_u(t) + \gamma r_u(t+1) + \dots + \gamma^{T-t+1} r_u(T-1) + \gamma^{T-t} V(s_T) \quad (30)$$

where γ is the discount factor that determines the weight of future rewards, $V(s_t)$ is the state value function at state s_t , representing the expected return starting from state s_t . $r_u(t)$ is the reward received at time step t , T is the final time step in the episode, and s_T is the state at the final time step T . The Total loss is expressed as

$$L_{\text{total}}(\theta) = \hat{\mathbb{E}}_t \left[L_t^{CLIP}(\theta) - c_1 L_t^{VF}(\theta) + c_2 S[\pi_\theta](s_t) \right] \quad (31)$$

where c_1, c_2 are coefficients used for exploitation and exploration respectively, and S denotes an entropy bonus, and L_t^{VF} is a squared-error loss $(V_\theta(s_t) - V_t^{\text{targ}})^2$. Algorithm 1 illustrates the PPO approach for both TDD and FDD³.

V. NUMERICAL RESULTS

We begin by outlining the assumptions and system configuration of our simulations, including the environment parameters and grid world setup. The problem is addressed using the PPO algorithm to evaluate the performance of both 3D-FDD and 2D-TDD approaches. We compare the results obtained from the proposed RL approaches with benchmark methods, such as RW, RR, and GA, to highlight the improvements and effectiveness of the proposed solutions.

³For simplicity, we present the two algorithms combined here. However, it is important to note that each algorithm is fundamentally different from the other. The key distinction lies in their action spaces, resulting in differing dimensions. Furthermore, each algorithm has its own set of penalty terms and requires separate hyperparameter tuning (such as discount factor γ and learning rate α) to achieve optimal performance.

Algorithm 1: PPO for TDD and FDD

Input: Environment with locations of IoUT nodes c_k , AUV starting position $l_{aUV}(0)$, AoI for all nodes $A(0)$, other parameters (i.e, operating frequencies, etc..)

1 . Output: Trained PPO agent

2 Initialization:

3 Initialize PPO agent π_θ , value network V_θ

4 Set training parameters: $max_episodes$, $max_iterations$...,

5 Procedure of Training:

6 **for** each episode $i = 1$ to $max_episodes$ **do**

7 $t \leftarrow 0$

8 Reset environment: l_{aUV} , $A(t)$, $\mathcal{E}(t)$ and set $max_iterations$

9 Initialize cumulative reward $R \leftarrow 0$

10 **while** $max_iterations > 0$ **do**

11 $t \leftarrow t + 1$

12 $max_iterations \leftarrow max_iterations - 1$

13 **Action Selection:**

14 Observe state $s(t)$

15 **if** TDD **then**

16 | Sample action $a_t = \{d(t), I(t) = W(t)\}$

17 **else**

18 | Sample action $a_t = \{d(t), I(t), W(t)\}$

19 **end**

20 **Environment Interaction:**

21 Move AUV according to the direction from a_τ .

22 Compute harvested energy and update AoI for the selected node(s) using (20),(19),(21).

23 **Reward Calculation:**

24 Compute discrimination index using (22).

25 Compute reward $r_u(t)$ and penalize unfair AoI distribution and wasted energy according to the mode selected (FDD or TDD) using equations (23), (25), (26), (27), and (28).

26 **Learning:**

27 Store (s_t, a_t, r_t, s_{t+1}) in buffer

28 **if** buffer full **then**

29 | Update PPO policy π_θ and value function V_θ .

30 **end**

31 Update cumulative reward

32 **end**

33 **end**

36 Procedure of Testing:

37 Load trained policy π_θ and evaluate on the test environment.

38 Simulate AUV operation and measure cumulative reward, fairness, AoI reduction.

1) *Simulation parameters:* In this study, we assumed a 3D grid for our simulations to better represent real-world underwater environments, which often involve a vertical dimension critical to communication and navigation. This choice adds complexity compared to the commonly used 2D grids,

TABLE I
THE SIMULATION PARAMETERS

Parameter	Value
Network size	$1000 \text{ m} \times 1000 \text{ m} \times 400 \text{ m}$
Electrical power (P_{elec})	2000 Watts
FDD Mode Frequency:	Inf transmission: 30 kHz Energy harvesting: 40 kHz
TDD Mode Frequency:	40 kHz
Elect-acoustic coefficient (η)	0.5
Directivity index (DI)	20 dB
Sensitivity (RVS)	$-150 \text{ dB re V}/\mu\text{Pa}$
Speed of AUV (V)	4 m/s
Spreading factor (k_s)	1.5
Resistance (R_p)	125Ω
Packet size (L_t)	100 bytes
Bandwidth (B)	3000 Hz
Total navigation time (T)	2500 s
Noise power (NL)	30 dB
Minimum Fairness (J_{Tmin})	0.85
Maximum Age (A_{max})	50

making the simulations more realistic. The grid size is set to $1000 \text{ m} \times 1000 \text{ m} \times 400 \text{ m}$, reflecting a reasonable approximation. It is discretized by a cell size of 100 m, resulting in 400 unique geometric positions. The AUV begins at the center of this grid and communicates with K sensor nodes, where $K \in \{3, 5, 7, 10\}$. The main simulation parameters are depicted in Table I.

2) *Algorithm architecture and hyperparameter settings:* For training, we employed the PPO algorithm inspired by the one implemented in the Stable Baselines3 library. The neural network architecture consists of two fully connected layers with 64 neurons each, using Tanh activation functions. To ensure consistency across varying network sizes ($K \in \{3, 5, 7, 10\}$), we tuned the hyperparameters using grid search. Our goal was to identify a single set of hyperparameters for both algorithms (3D-FDD and 2D-TDD). The selected hyperparameters are summarized in Table II.

As illustrated in Algorithm 1, both techniques (TDD and FDD) share a similar RL environment in terms of the state space. However, they differ in the action space and reward function, as defined in equations (18),(17),(28) and (27). This distinction in the action space allows the agent to choose different actions (i.e., direction and node selection) depending on the duplexing technique adopted. The reward function is also adjusted accordingly to reflect the differences in energy transfer and AoI optimization.

TABLE II
HYPERPARAMETER SETTINGS FOR 2D-TDD AND 3D-FDD

Hyperparameter	2D-TDD	3D-FDD
Discount factor (γ)	0.93	0.92
Learning rate (α)	0.0003	0.0005
Entropy coefficient (c_2)	0.01	0.01
Batch size	100	100
Steps per update (n_{steps})	100	100

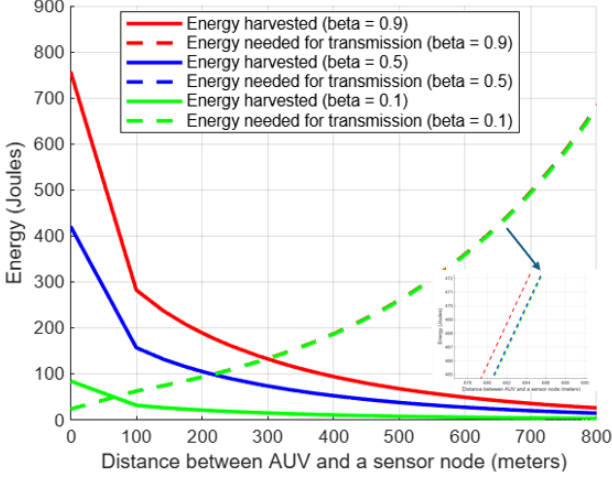


Fig. 4. Energy harvested and information uplink for different Values of β and for frequency $f = 40$ KHz.

3) *TDD mode configuration*: In Fig. 4, we analyze the TDD energy dynamics in the underwater communication system by examining the energy harvested and the energy required for information transmission across different values of β at a frequency of 40 KHz. The plot demonstrates that for $\beta = 0.1$, the energy harvested is the lowest, as only a small portion of time is dedicated to energy harvesting. This configuration may lead to challenges in maintaining efficient long-distance transmission due to insufficient energy harvesting. As β increases to 0.5 and 0.9, the energy harvested significantly rises, highlighting the direct impact of β on energy allocation. In these scenarios, more time is dedicated to energy harvesting, allowing the AUV to sustain longer energy transmission effectively. Notably, the energy needed for transmission remains relatively unaffected by variations in β . The observation that E_{trans} remains almost constant across different values of β is further explained in Appendix A.

Efficient simultaneous AET and information uplink operation is achieved when the energy harvested surpasses the energy required for transmission (i.e., the intersection points in Fig. 4). This critical condition is more likely to occur when β is higher, and the distance between the AUV and the IoT node is short. To further explore the optimization of β , Fig. 5 presents the relationship between β^* and the distance d^* for various communication frequencies which are the values of β and d that achieves the intersection in the Fig. 4. Here, we observe that β^* values ranging from 0 to 1 are achieved over shorter distances as the communication frequency increases. For instance, at higher frequencies such as 60 KHz, β^* quickly approaches its maximum value, reflecting a rapid signal attenuation requiring more charging time for reliable signal transmission.

Conversely, for lower frequencies, such as 10 KHz, β^* increases slowly with distance, supporting long-range AET and information uplink. This observation aligns with the goal of achieving a balanced configuration that supports both data transmission and energy harvesting, highlighting why a frequency of 40 KHz was selected in our next simulations. This

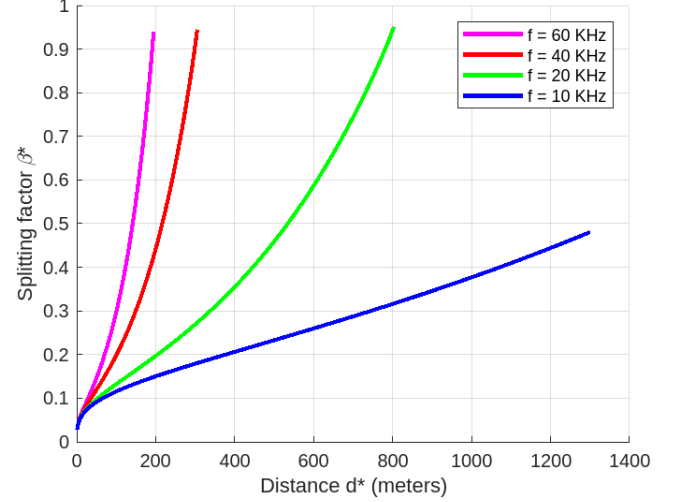


Fig. 5. Plot of β^* as a function of d^* for different frequencies

medium frequency enables a practical compromise, optimizing the trajectory of the AUV by extending the range and reducing antenna size while maintaining adequate bandwidth for data and energy transfer.

Herein, we choose to restrict β between 0.1 and 0.9 because practically, if the splitting factor is less than 0.1 (i.e., indicating that the charging time is less than 10%), there will not be enough time for AET, and only information uplink occurs. Conversely, if the splitting factor exceeds 0.9 ($\beta > 0.9$), only charging occurs, with insufficient time for information uplink. In addition to the observations from Fig. 5, we provide a rigorous mathematical treatment of how β is directly related to the distance d through an inequality. This is required for simultaneous AET and information uplink to occur, ensuring that energy harvesting is sufficient for data transmission. The relationship between β and d is formalized in Appendix B, where we analyze the sufficient condition

$$E_{\text{harv}} \geq E_{\text{req},k}, \quad (32)$$

which leads to

$$g(\beta) \geq h(d), \quad (33)$$

where $g(\beta)$ and $h(d)$ are derived from energy harvesting and transmission models, as detailed in Appendix B.

By proving the function $g(\beta)$ is bijective within the interval $\beta_1 < \beta < \beta_2$, where β_1 is close to 0 and β_2 is close to 1 as shown in Appendix B, we demonstrate that β is strictly increasing with d , implying a direct relationship. This bijection ensures that for any distance d^* , there exists a unique β^* , supporting our selection of frequencies and configurations in the simultaneous AET and information uplink process in TDD.

4) *Performance Evaluation*: The plot in Fig. 6 illustrates the average AoI for various number of IoT nodes using different AUV trajectory optimization and scheduling methods. The RW method, represented by the blue dashed line, shows the highest AoI across all nodes, indicating its inefficiency in maintaining up-to-date information. The RR method performs better than RW, reducing the AoI by approximately 16% for

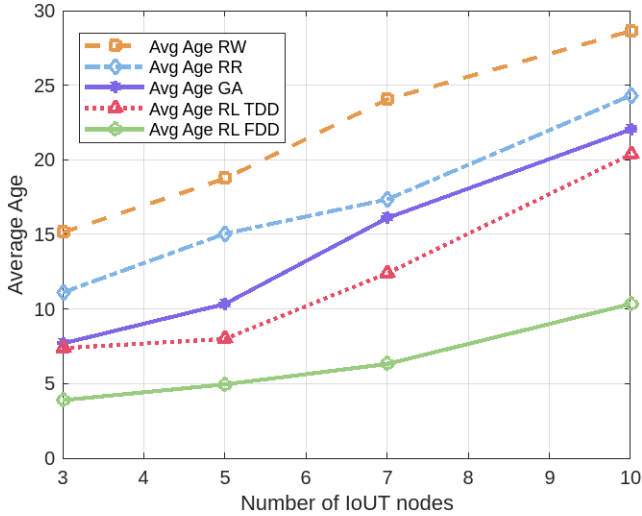


Fig. 6. Average AoI for different algorithms and network sizes.

small number of nodes and up to 25% for a higher number of nodes (i.e., 7 and 10). The GA further reduces the AoI compared to RR, especially for lower-number of nodes with a reduction of approximately 30%. This reflects that positioning the AUV near the center of gravity manages to solve the optimization problem more efficiently, but of course at the cost of fairness. In contrast, our RL based approaches, both 2D-TDD and 3D-TDD, demonstrate significant improvements over the GA and RR methods. The 2D-TDD achieves a lower AoI than GA, reducing it by about 15.5%, which highlights its effectiveness in optimizing the AUV's path. The best performance is observed for the 3D-TDD, which maintains a consistently low AoI across all nodes to showcase its superior efficiency in terms of AoI reduction over all other methods.

Looking at Fig. 7, we notice that both RW and RR methods render similar and relatively low energy harvesting capabilities across all node counts (i.e., not exceeding 7 KJ). This indicates their inefficiency in energy management. The proposed RL approaches with 2D-TDD and 3D-FDD action spaces demonstrate significant improvements over the RW, RR, and GA methods. The RL with a 2D-TDD action space harvests an amount ranging from 8 KJ to 9.2 KJ. However, its performance is inferior to the 3D-TDD (green bars), which achieves the highest energy harvesting levels among all methods across all different network sizes, indicating its superiority as expected. The RL 3D-FDD method harvests more than 10.5 KJ in all cases and up to 11.7 KJ in the 7-node setup. This highlights the 3D-FDD approach's effectiveness and superiority in energy harvesting by dynamically adjusting to the environment. We can further explore the efficiency of 3D-FDD in Fig. 8, where it consistently maintains the highest fairness index outperforming 2D-TDD, which leads to a quasi-uniform distribution of resources across all nodes. In contrast, the benchmark methods exhibit increased randomness for a higher number of IoT devices, resulting in lower fairness as shown in the figure.

5) *Complexity Evaluation:* The environmental impact of training ML models has become a significant concern within the ML community due to their substantial energy consump-

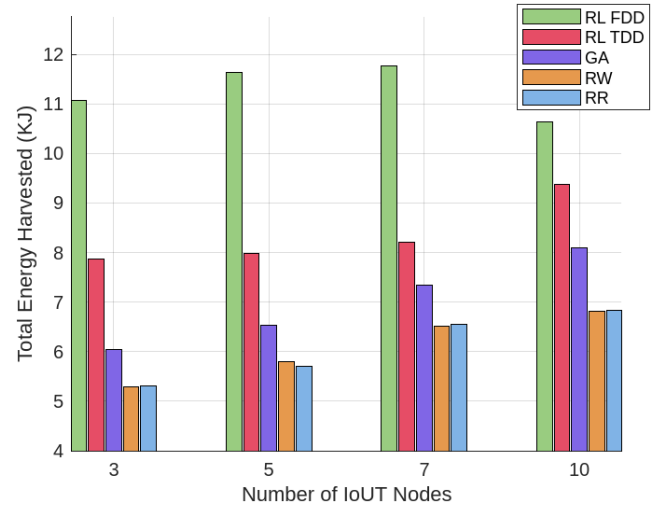


Fig. 7. Total energy harvested plot for different algorithms and network sizes.

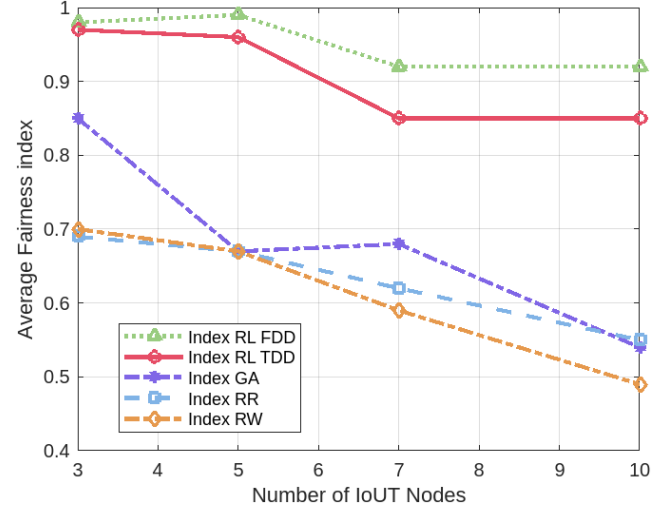


Fig. 8. The average Jain's fairness index for different algorithms and network sizes

tion and carbon emissions. The eco2ai library introduced in [27] addresses this issue by providing a tool to track AI models' carbon footprint and energy consumption during both the training and inference phases, promoting sustainable practices in AI development. In our work, we adopt eco2ai to compare the 2D-TDD to 3D-FDD. Table. III highlights that models with more IoT nodes generally require longer training times, leading to higher energy consumption and more CO₂ emissions. The consistent use of the same hardware (i.e., CPU: AMD Ryzen 7 5800H with Radeon Graphics; GPU: NVIDIA GeForce GTX 1650) across all models ensures that these variations are primarily due to differences in model configurations and training times. Notably, the model that adopts 2D-TDD consistently consumes less energy and emits less CO₂ compared to their 3D-FDD counterparts, indicating a lower environmental impact for simpler models.

While the current study is based on simulations, the proposed solutions can be tested in real-world scenarios to validate their applicability further. Specifically, the framework

TABLE III
A COMPLEXITY ANALYSIS AND ENVIRONMENTAL IMPACT FOR THE PROPOSED METHODS.

PPO Model	Train Time	Energy (kWh)	CO2 (kg)
3 nodes TDD	58 min	0.0173	0.0099
3 nodes FDD	1 h 9 min	0.0188	0.0107
5 nodes TDD	1 h 24 min	0.0231	0.0132
5 nodes FDD	2 h 17 min	0.0838	0.0478
7 nodes TDD	3 h 34 min	0.1382	0.0788
7 nodes FDD	6 h 4 min	0.2174	0.1240
10 nodes TDD	6 h 47 min	0.2246	0.1260
10 nodes FDD	8 h 11 min	0.2942	0.1679

can be implemented in a controlled underwater testbed using AUVs equipped with acoustic modems for communication and energy transfer modules. Such an experimental setup would allow us to evaluate the practical feasibility of the FDD and TDD schemes under varying underwater conditions, including different water depths, noise levels, and environmental factors.

VI. CONCLUSIONS

This paper proposed two RL schemes for simultaneous AET and information uplink in IoUT network via AUV. The first scheme is FDD, which shows high performance in terms of age minimization and energy harvesting at the cost of higher complexity and hardware cost. The second scheme is TDD which offers a sub-optimal performance at lower complexity, less Co2 emissions and hardware cost. The results demonstrated that both schemes significantly improved energy harvesting efficiency, data collection, and fairness in resource distribution compared to conventional RW, GA, RR benchmarks.

Future work may include accounting for the AUV navigation energy and the deployment of multiple AUVs to serve massive IoUT networks via multi-agent reinforcement learning and meta-learning for dynamic environments. Reconfigurable intelligent surfaces (RIS) could be also applied in underwater environments to boost the efficiency of AET and information uplink in the same way it is deployed in terrestrial and non-terrestrial networks [28].

APPENDIX A

DEMONSTRATING HOW $E_{req,k}$ IS ALMOST CONSTANT

In this appendix, we provide a detailed explanation for why the energy needed for transmission, $E_{req,k}$, remains relatively unaffected by changes in β . We start with the expression for $E_{req,k}$

$$E_{req,k} = P_{trans,k} \cdot (1 - \beta) \cdot \tau. \quad (34)$$

Using (12)

$$E_{req,k} = \gamma_k \cdot 10^{\frac{AL+NL}{10}} \cdot (1 - \beta) \cdot \tau. \quad (35)$$

Referring to (11), we can write the throughput as

$$S = \frac{L_t}{(1 - \beta) \cdot \tau}, \quad (36)$$

where L_t is the packet size, indicating the quantity of data per transmission

Hence,

$$E_{req,k} = \left(2^{\left(\frac{L_t}{(1 - \beta) \cdot \tau \cdot B} \right)} - 1 \right) \cdot 10^{\frac{AL+NL}{10}} \cdot (1 - \beta) \cdot \tau. \quad (37)$$

Using the Taylor expansion, we can deduce that

$$2^{\left(\frac{L_t}{(1 - \beta) \cdot \tau \cdot B} \right)} \approx 1 + \frac{L_t \cdot \log(2)}{(1 - \beta) \cdot \tau \cdot B}. \quad (38)$$

Therefore,

$$E_{req,k} \approx \frac{L_t \cdot \log 2}{(1 - \beta) \cdot \tau \cdot B} \cdot 10^{\frac{AL+NL}{10}} \cdot (1 - \beta) \cdot \tau \quad (39)$$

Simplifying, we obtain

$$E_{req,k}(\beta, d) \approx E_{req,k}(d) = \frac{L_t \cdot \log 2}{B} \times 10^{\frac{AL(d)+NL}{10}}. \quad (40)$$

Now, let $K = \frac{L_t \cdot \log(2)}{B} \cdot 10^{\frac{NL}{10}}$. We attain

$$E_{req,k}(d) \approx K \cdot 10^{\frac{AL(d)}{10}}. \quad (41)$$

Plugging the values indicated in TABLE II, we end up with

$$E_{req,k}(d) \approx 23.105 \times 10^{\frac{AL(d)}{10}}. \quad (42)$$

Thus, the energy required for transmission is approximately constant due to the significant effect of the constant term in the power calculation and the nearly linear dependency of the SNR on $(1 - \beta)$. From Table IV, we can observe the tightness of the proposed approximation, where the normalized mean square error is in the order of 10^{-5} for all values of β and d .

TABLE IV
A COMPARISON OF TRUE AND APPROXIMATED ENERGY VALUES.

Distance (d)	Approximated Energy (J) (42)	True Energy (J) (37)		
		$\beta = 0.1$	$\beta = 0.5$	$\beta = 0.9$
100	62.0503	62.0819	62.1075	62.3377
200	92.6695	92.7167	92.7548	93.0986
300	132.5527	132.6202	132.6747	133.1665
700	494.0117	494.2635	494.4666	496.2996
800	678.3817	678.7274	679.0063	681.5234
900	929.3624	929.8360	930.2181	933.6665

APPENDIX B

ENERGY HARVESTING VS ENERGY REQUIRED FOR TRANSMISSION

We explore the relationship between β and d , ensuring that energy harvesting is sufficient for reliable data transmission.

1) *Energy harvested*: Assuming β amount of time for energy harvesting and using (1) in (9), we obtain

$$\begin{aligned} E_{harv} &= \beta \cdot \tau \cdot P_{harv} \\ &= \beta \cdot \tau \cdot \frac{\eta}{4R_p} 10^{\frac{RVS+RL}{10}} \\ &= \beta \cdot \tau \cdot K_2 \cdot 10^{-\frac{AL}{10}}, \end{aligned} \quad (43)$$

where $K_2 = \frac{\eta}{4R_p} 10^{\frac{RVS+SL-NL}{10}}$.

2) *Energy required for transmission:* Assuming $1 - \beta$ portion of time for information uplink, from (37) we have

$$E_{req,k} = \left(2^{\left(\frac{L_t}{(1-\beta) \cdot \tau \cdot B} \right)} - 1 \right) \times 10^{\frac{AL+NL}{10}} \times (1 - \beta) \cdot \tau. \quad (44)$$

3) *Inequality Comparison:* In order to perform successful transmission, the harvested energy must be greater than or equal to the amount of energy required for the information uplink. That is

$$E_{harv} \geq E_{req,k}, \quad (45)$$

Plugging (44) and (45), the inequality gives

$$\beta \cdot \kappa_2 \cdot 10^{-\frac{AL}{10}} \geq (1 - \beta) \cdot \left(2^{\frac{L_t}{(1-\beta) \cdot \tau \cdot B}} - 1 \right) \cdot 10^{\frac{AL+NL}{10}} \quad (46)$$

leading to

$$\frac{\beta \cdot \kappa_3}{(1 - \beta) \left(2^{\frac{L_t}{(1-\beta) \cdot \tau \cdot B}} - 1 \right)} \geq 10^{\frac{AL}{5}}, \quad \kappa_3 = \kappa_2 \cdot 10^{-\frac{NL}{10}} \quad (47)$$

Taking logarithm base 10 for both sides, we attain

$$\log_{10} \left(\frac{\beta}{1 - \beta} \right) - \log_{10} \left(2^{\frac{L_t}{(1-\beta) \cdot \tau \cdot B}} - 1 \right) \geq \frac{AL}{5} - \log_{10} \kappa_3, \quad (48)$$

where

$$AL(d) = k_s \cdot \log_{10}(d) + \kappa_4 \cdot d \quad \text{with} \quad \kappa_4 = \alpha(f). \quad (49)$$

Finally,

$$\begin{aligned} \log_{10} \left(\frac{\beta}{1 - \beta} \right) - \log_{10} \left(2^{\frac{L_t}{(1-\beta) \cdot \tau \cdot B}} - 1 \right) &\geq \\ k_s \log_{10}(d) + \frac{\kappa_4 d}{5} - \log_{10} \kappa_3. \end{aligned} \quad (50)$$

Hence,

$$g(\beta) \geq h(d), \quad (51)$$

where

$$g(\beta) = \log_{10} \left(\frac{\beta}{1 - \beta} \right) - \log_{10} \left(2^{\frac{L_t}{(1-\beta) \cdot \tau \cdot B}} - 1 \right) \quad (52)$$

$$h(d) = \frac{1}{5} (k_s \log_{10}(d) + \kappa_4 \cdot d) - \log_{10} \kappa_3 \quad (53)$$

4) *Derivative Calculation:* The derivation of $g(\beta)$ with respect to β gives

$$\begin{aligned} \frac{\partial g}{\partial \beta} &= \frac{1}{\log 10} \left(\frac{1}{\beta(1 - \beta)} \right. \\ &\quad \left. + \frac{2^{\frac{L_t}{(1-\beta) \cdot \tau \cdot B}} \log 2 \cdot \left(\frac{L_t}{(1-\beta)^2 \cdot \tau \cdot B} \right)}{2^{\frac{L_t}{(1-\beta) \cdot \tau \cdot B}} - 1} \right). \end{aligned} \quad (54)$$

Proof of Bijectivity: To prove the bijectivity of $g(\beta)$, we need to prove its injectivity and surjectivity within the domain $\beta \in [\beta_1, \beta_2]$ where β_1 is close to 0 and β_2 is close to 1. To prove injectivity, we examine the derivative of $g(\beta)$. Since $\beta \in [\beta_1, \beta_2]$, both β and $1 - \beta$ are positive, making $\frac{1}{\beta(1-\beta)} > 0$. For the second term, the expression $\frac{L_t}{(1-\beta)^2 \cdot \tau \cdot B} > 0$ since L_t, τ, B are all positive. Therefore, $2^{\frac{L_t}{(1-\beta) \cdot \tau \cdot B}} > 1$, which implies that both the numerator $2^{\frac{L_t}{(1-\beta) \cdot \tau \cdot B}} \cdot \log(2) \cdot \left(\frac{L_t}{(1-\beta)^2 \cdot \tau \cdot B} \right)$ and

the denominator $2^{\frac{L_t}{(1-\beta) \cdot \tau \cdot B}} - 1$ are positive. Hence, the overall derivative $\frac{\partial g}{\partial \beta} > 0$ in the interval $\beta \in [\beta_1, \beta_2]$, confirming that g is strictly increasing and injective in the interval $\beta \in [\beta_1, \beta_2]$.

Proof of Surjectivity: Since $g(\beta)$ is continuous by definition of logarithmic function, and strictly increasing in the interval $\beta \in [\beta_1, \beta_2]$, it will cover all values between its minimum and maximum, $g(\beta_1)$ and $g(\beta_2)$. Therefore, g is surjective onto its range.

Since g is both injective and surjective in the interval $\beta \in [\beta_1, \beta_2]$, we conclude that $g(\beta)$ is bijective in this interval.

REFERENCES

- [1] D. Centelles *et al.*, "Wireless RF camera monitoring for underwater cooperative robotic archaeological applications," *Instrumentation viewpoint*, no. 18, pp. 51–52, 2015.
- [2] H. Guo and A. A. Ofori, "The internet of things in extreme environments using low-power long-range near field communication," *IEEE Internet of Things Magazine*, vol. 4, no. 1, pp. 34–38, 2021.
- [3] T. Ahmad, X. J. Li, A. K. Cherukuri, and K.-I. Kim, "Hierarchical localization algorithm for sustainable ocean health in large-scale underwater wireless sensor networks," *Sustainable Computing: Informatics and Systems*, vol. 39, p. 100902, 2023. [Online]. Available: <https://www.sciencedirect.com/science/article/pii/S2210537923000574>
- [4] S. Reddy, R. Arya, and Prateek, "Compensation of coordinated attacks in underwater internet of sensor networks," *IEEE Transactions on Consumer Electronics*, vol. PP, pp. 1–1, 08 2024.
- [5] B. Shihada *et al.*, "Aqua-fi: Delivering internet underwater using wireless optical networks," *IEEE Communications Magazine*, vol. 58, no. 5, pp. 84–89, 2020.
- [6] A. Eid *et al.*, "Enabling long-range underwater backscatter via van atta acoustic networks," in *Proceedings of the ACM SIGCOMM 2023 Conference*, 2023, pp. 1–19.
- [7] E. Saifeer, S. Tahir, M. Shaheen, and M. S. Farooq, *Federated Learning for Internet of Underwater Drone Things*. Cham: Springer Nature Switzerland, 2024, pp. 295–309. [Online]. Available: https://doi.org/10.1007/978-3-031-64642-3_13
- [8] A. Pal *et al.*, "Communication for underwater sensor networks: A comprehensive summary," *ACM Transactions on Sensor Networks*, vol. 19, no. 1, pp. 1–44, 2022.
- [9] A. Wibisono, M. H. Alsharif, H.-K. Song, and B. M. Lee, "A survey on underwater wireless power and data transfer system," *IEEE Access*, vol. 12, pp. 34942–34957, 2024.
- [10] R. Guida, E. Demirors, N. Dave, and T. Melodia, "Underwater ultrasonic wireless power transfer: A battery-less platform for the internet of underwater things," *IEEE Transactions on Mobile Computing*, vol. 21, no. 5, pp. 1861–1873, 2022.
- [11] M. Y. I. Zia, J. Poncela, and P. Otero, "State-of-the-art underwater acoustic communication modems: Classifications, analyses and design challenges," *Wireless personal communications*, vol. 116, pp. 1325–1360, 2021.
- [12] M. Jouhari, K. Ibrahimi, H. Tembine, and J. Ben-Othman, "Underwater wireless sensor networks: A survey on enabling technologies, localization protocols, and internet of underwater things," *IEEE Access*, vol. 7, pp. 96879–96899, 2019.
- [13] Y. Zhao *et al.*, "Design of ultrasonic transducer structure for underwater wireless power transfer system," in *2021 IEEE Wireless Power Transfer Conference (WPTC)*, 2021, pp. 1–4.
- [14] A. Kosta, N. Pappas, and V. Angelakis, "Age of information: A new concept, metric, and tool," *Foundations and Trends in Networking, Now Publishers, Inc.*, 2017.
- [15] Y. Ma *et al.*, "Improving age of information for covert communication with time-modulated arrays," *IEEE Internet of Things Journal (early access)*, pp. 1–1, 2024.
- [16] M. A. Abd-Elmagid, A. Ferdowsi, H. S. Dhillon, and W. Saad, "Deep Reinforcement Learning for Minimizing Age-of-Information in UAV-Assisted Networks," in *2019 IEEE Global Communications Conference (GLOBECOM)*, 2019, pp. 1–6.
- [17] E. Eldeeb *et al.*, "Multi-uav path learning for age and power optimization in iot with uav battery recharge," *IEEE Transactions on Vehicular Technology*, vol. 72, no. 4, pp. 5356–5360, 2023.

- [18] E. Eldeeb, M. Shehab, and H. Alves, "Age minimization in massive iot via uav swarm: A multi-agent reinforcement learning approach," in *2023 IEEE 34th Annual International Symposium on Personal, Indoor and Mobile Radio Communications (PIMRC)*, 2023, pp. 1–6.
- [19] K. G. Omeke *et al.*, "Toward a sustainable internet of underwater things based on auvs, swipt, and reinforcement learning," *IEEE Internet of Things Journal*, vol. 11, no. 5, pp. 7640–7651, 2024.
- [20] ———, "How reinforcement learning is helping to solve internet-of-underwater-things problems," *IEEE Internet of Things Magazine*, vol. 5, no. 4, pp. 24–29, 2022.
- [21] J. Dai *et al.*, "Relay selection and power control for mobile underwater acoustic communication networks: A dual-thread reinforcement learning approach," *IEEE Transactions on Green Communications and Networking*, pp. 1–1, 2024.
- [22] A. Bereketi and S. Bilgen, "Remotely powered underwater acoustic sensor networks," *IEEE Sensors Journal*, vol. 12, no. 12, pp. 3467–3472, 2012.
- [23] A. Ahmadian and H. Park, "Wireless Powered Communication Networks: TDD or FDD?" 2018. [Online]. Available: <https://arxiv.org/abs/1807.05670>
- [24] Y. He, Y. Gan, H. Cui, and M. Guizani, "Fairness-based 3-d multi-uav trajectory optimization in multi-uav-assisted mec system," *IEEE Internet of Things Journal*, vol. 10, no. 13, pp. 11 383–11 395, 2023.
- [25] H. Farag, M. Gidlund, and C. Stefanovic, "A deep reinforcement learning approach for improving age of information in mission-critical iot," in *2021 IEEE Global Conference on Artificial Intelligence and Internet of Things (GCAIoT)*, 2021, pp. 14–18.
- [26] J. Schulman *et al.*, "Proximal policy optimization algorithms," 2017. [Online]. Available: <https://arxiv.org/abs/1707.06347>
- [27] S. A. Budennyy *et al.*, "Eco2AI: carbon emissions tracking of machine learning models as the first step towards sustainable AI," in *Doklady Mathematics*, vol. 106, no. Suppl 1. Springer, 2022, pp. S118–S128.
- [28] K. An *et al.*, "Exploiting multi-layer refracting ris-assisted receiver for hap-swipt networks," *IEEE Transactions on Wireless Communications*, vol. 23, no. 10, pp. 12 638–12 657, 2024.